BINARY AND TERNARY MOLECULES BLEND BULK HETEROJUNCTION ORGANIC SOLAR CELL

MSc Dissertation

by

Emmanuel Khulekani Mkhwanazi

Under the supervision of

Prof. Genene Tessema Mola

Pietermaritzburg Campus, South Africa

2015

BINARY AND TERNARY MOLECULES BLEND BULK HETEROJUNCTION ORGANIC SOLAR CELL

MSc Dissertation

by

Emmanuel Khulekani Mkhwanazi

Under the supervision of

Prof. Genene Tessema Mola

Submitted in fulfilment of the academic requirements of Master of Science

in Physics

School of Chemistry and Physics

Collage of Agriculture, Engineering and Science

University of KwaZulu-Natal

Pietermaritzburg

South Africa

November 2015

0.1 PREFACE

The research contained in this dissertation was completed by the candidate while based in the Discipline of Physics, School of Chemistry and Physics of the College of Agriculture, Engineering and Science, University of KwaZulu-Natal, Pietermaritzburg, South Africa. The research was financially supported by National Research Foundation(NRF).

The contents of this work have not been submitted in any form to another university and, except where the work of others is acknowledged in the text, the results reported are due to investigations by the candidate.

Signed: _____ Name: _____

Date: _____

0.2 DECLARATION : PLAGIARISM

I, Emmanuel Khulekani Mkhwanazi, declare that:

(i) the research reported in this dissertation, except where otherwise indicated or acknowledged, is my original work;

(ii) this dissertation has not been submitted in full or in part for any degree or examination to any other university;

(iii) this dissertation does not contain other persons data, pictures, graphs or other information, unless specifically acknowledged as being sourced from other persons;

(iv) this dissertation does not contain other persons writing, unless specifically acknowledged as being sourced from other researchers. Where other written sources have been quoted, then:

a) their words have been re-written but the general information attributed to them has been referenced;

b) where their exact words have been used, their writing has been placed inside quotation marks, and referenced;

(v) where I have used material for which publications followed, I have indicated in detail my role in the work;

(vi) this dissertation is primarily a collection of material, prepared by myself, published as journal articles or presented as a poster and oral presentations at conferences. In some cases, additional material has been included;

(vii) this dissertation does not contain text, graphics or tables copied and pasted from the Internet, unless specifically acknowledged, and the source being detailed in the dissertation and in the References sections.

Signed: _____

0.3 Abstract

Bulk heterojunction organic solar cells were prepared and characterized in terms of electrical and optical properties of the photosensitive medium. Two cases of organic solar cells were developed in this investigation with active layers composed of P3HT:PCBM molecules blend and P3HT:PTB7:PCBM ternary molecules blend, at stoichiometric ratio 1:1 and 2:1:1, respectively. The ternary molecules blend active layer attracted the attention of the researchers because of the possibility of broadening the absorption band. The performance of the devices was investigated and found better device performance in binary molecules blend while low charge mobility was observed in the ternary molecules blend active layer. The highest power conversion efficiency (η) obtained were 1.6 % for P3HT:PCBM blend and 0.56 % for P3HT:PTB7:PCBM active layer. The result indicated that the charge transfer mechanisms in the ternary molecules blend were not favorable on the extraction and transportation of charges to the electrodes. The morphologies of the films and charge transfer properties in the two media are discussed based on SEM images and electrical measurements.

0.4 Acknowledgments

It got me the full two years to finish my Masters dissertation, during that two years there was challenges that could have taken in me dont go forward with my Masters, but lastly I got this far. Thus, I will like to first thank God for keeping me awake and feeding me the strength to face all the challenges I had come across. Secondly, my supervisor Prof. Genene Tessema Mola whose assistance and guidance is very much appreciated because without him this work would not be finished on time. His encouragement helps me to focus and understand the field of semiconductors and solar cells. Thirdly, all my family members are thankful for their support and encouragement towards everything in my entire lifetime. Fourthly, the financial assistance of the National Research Foundation (NRF) towards this research is hereby acknowledged. Lastly, the School of Chemistry and Physics is also recognized for offering a very conducive place to manage the research work.

Contents

List of Figures

List of Tables

Chapter 1

Introduction

1.1 Historical background of OPV

Organic semiconductors have become interesting materials for photovoltaic (PV) and light emitting diodes (LEDs) applications. There have been extremely great efforts made in the synthesis and characterizations of organic semiconductor molecules in the last two decades [1, 2]. The branch of organic photovoltaic (OPV) research emerged after the discovery of several organic semiconductor molecules were available for device fabrication [3]. The long polymer chains were chemically polymerized using smaller monomer units which notably improved the charge transport mechanism on the backbone of the largest polymer molecules.

The difference between the organic and inorganic semiconductors is due to the poor charge-carrier mobility of organic semiconductor medium than the inorganic counter part. This has highly affected the design and efficiency of organic semiconductor devices. However, the low mobility in the organic semiconductors is partially compensated by its strong photon absorption co-

efficients (usually $\geqslant 10^5\ cm^{-1}$) which assists to enhance the creation of charge carriers in the medium [4]. Even the thin film layer of polymer molecules (< 100 nm) has a high absorption coefficient. Organic semiconductors have many advantages over the inorganic counterpart such as: low device fabrication cost, mechanical flexibility and light weight. Because of such attractive properties, organic semiconductors were employed to fabricate low cost photovoltaic cells. Furthermore, they are less energy consuming devices. Since the 1990's, several research works have been performed with the aim of producing efficient and low cost OPV cells, but the power conversion efficiencies achieved are low compared to semiconductors based solar cells.

The first OPV solar cell was fabricated based on a single layer device structure which was sandwitched between two metal electrodes consisting of different work functions [1, 3]. The power conversion efficiency (η) of the first OPVs was reported to be generally poor ($\simeq 10^{-3} - 10^{-2}$ %). An organic bilayer was then introduced to solve the problems observed in the single layer solar cell. In bilayer devices, p-and n-type organic semiconductor layers were arranged one over the other and sandwitched between the electrodes. The junction of these two layers forms a zone of charge separation regions where the free charge carriers are transported in the two different layers to the opposite electrodes. In 1986, η about 1 % was reported by Tang for two organic materials using bilayer device architecture [5]. This device structure was good for many years up until at the turn of the millennium. The most effective device structure to date is the bulk heterojunction devices introduced by Hiramoto and co-workers [6]. More details about device structures will be given in chapter 4.

In the last ten years, a renewed interest has been dedicated to OPV cells because of the progress attained so far. This new interest is motivated by two recent developments in the field of organic semiconductors. Firstly, it has shown that the quantum efficiency of the electron transfer from an excited polymer to C_{60} is very high and very fast [7], which is the necessary property for charge carrier separation in organic photovoltaic cells. Secondly, the realization of efficient organic electronic displays based on organic light emitting diodes (OLEDs). These fast development attracted several researchers into the field, both in academics and industry. The low cost technology is now used to develop those OLED displays and, currently, important progresses are under way to the realization of OPV solar cells [8].

1.2 Technological importance of OPV

OPV technology is among an attractive research field at present with the view to solve the energy challenges. Because of rapidly increasing energy demand, there is an intensive search for renewable and clean sources of energy. The OPV is one of the alternatives available at present which can harvest renewable and clean energy sources from solar radiation. The mechanical flexibility of OPVs allowed the potential uses in unfamiliar areas such as solar cells on electronic machines, clothing, windows and also there are some researchers who are suggesting about using OPVs as curtains. OPVs can generate power for a large portion of the day. However, η of OPVs is still far from silicon based solar cells to compete in the energy market. The following key advantages of OPV devices have been identified over other types of solar energy converter :

1. Low weight and flexibility of the PV modules,
2. Semi-transparency,
3. Easy integration into other products,
4. Significantly lower manufacturing costs compared to conventional inorganic technologies,
5. Short energy payback times and low environmental impact during manufacturing and operations.

Some of the advantages listed above applies also to solar cells based on vapor-deposited small molecule absorbers. This suggests that OPV does have a potential to be a new technology within the PV market. The research and development activities have been initiated and substantial progress has been made in improving η of solution processed OPV during last years.

Chapter 2

Theory of Charge Transport

2.1 Space Charge Limited Current

Mott and Gurney were the first to propose the theory of space charge limited current between two parallel electrodes. The current density in a conducting medium in the absence of any traps is given by the Mott-Gurney law [14]

$$J = \frac{9}{8}\mu\epsilon\epsilon_0\frac{V^2}{L^3} \tag{2.1}$$

Where μ is the free charge mobility, ϵ is the dielectric constant of the material, V is the applied voltage and L is the electrode separation distance. This current density is assumed to consist of the drift carriers only, the effect of diffusion is not included. Further assumption in equation 2.1 is that, the charge mobility is independent of the field. The theory of Space Charge Limited Current (SCLC) has been improved by several authors, Lambert at (1956) is one of those authors. Later in (1970), Murgatroyd derived a modified form of the current density equation 2.1 for the case of one set of traps located below the conduction band at energy level E_t (Fig. 2.1). Under this situation, and, in the presence of a significant amount of empty traps;

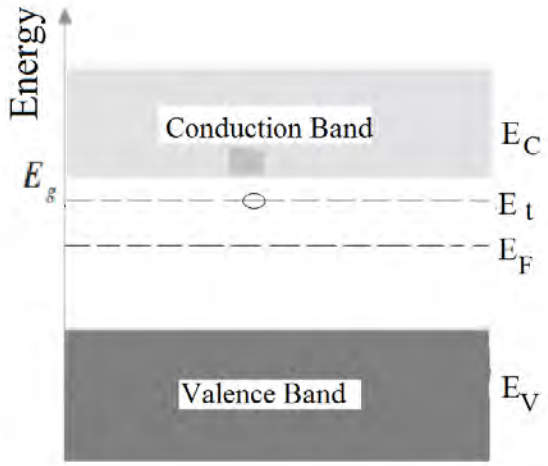

Figure 2.1: Single energy traps level in energy band gap.

the proportion of free total charge to empty traps is approximated by [14] as :

$$\frac{\rho_f}{\rho_f + \rho_t} = \frac{N_c}{N_t} exp(-\frac{A}{kT}) = \theta_0 \tag{2.2}$$

Where ρ_f is a free charge density, ρ_t is a trap charge density, N_c is the effective density of states in the conduction band and N_t is the density of traps. Since the diffusion effect is neglected, the current density is given by :

$$J = \mu \rho_f E \tag{2.3}$$

The Poisson's equation of the form :

$$\frac{dE}{dx} = \frac{\rho_f + \rho_t}{\epsilon \epsilon_0} \tag{2.4}$$

Can be re-arranged to acquire :

$$\rho_f + \rho_t = \epsilon \epsilon_0 \frac{dE}{dx} \tag{2.5}$$

By substituting equation 2.5 into equation 2.2 we get

$$\rho_f = \epsilon \epsilon_0 \theta_0 \frac{dE}{dx} \tag{2.6}$$

Substitution of equation 2.6 into equation 2.3 gives the current density as :

$$J = \mu\epsilon\epsilon_0\theta_0 E\frac{dE}{dx} \tag{2.7}$$

This equation can be re-arranged also to get :

$$\frac{Jdx}{\mu\epsilon\epsilon_0\theta_0} = EdE \tag{2.8}$$

The integration of equation 2.8 from 0 to x goes as follows :

$$\frac{J}{\mu\epsilon\epsilon_0\theta_0}\int_0^x dx = \int_{E(0)}^{E(x)} EdE \tag{2.9}$$

$$\frac{Jx}{\mu\epsilon\epsilon_0\theta_0} = \frac{1}{2}(E^2(x) - E^2(0)) \tag{2.10}$$

Assuming that the injecting electrode is at $x = 0$, therefore $E(0) = 0$ then solving E in equation 2.10 gives :

$$E = \sqrt{\frac{2Jx}{\mu\epsilon\epsilon_0\theta_0}} \tag{2.11}$$

Integrating equation 2.11 from 0 to L gives :

$$E\int_0^L dx = \sqrt{\frac{2J}{\mu\epsilon\epsilon_0\theta_0}}\int_0^L x^{\frac{1}{2}}dx \tag{2.12}$$

$$EL = \frac{2}{3}\Big(\frac{2J}{\mu\epsilon\epsilon_0\theta_0}\Big)^{\frac{1}{2}}L^{\frac{3}{2}} \tag{2.13}$$

Solving for the current density in equation 2.13 goes as follows, we square both sides of equation 2.13 and use $E = \frac{V}{L}$ the field between two electrodes :

$$E^2L^2 = \frac{4}{9}\Big(\frac{2J}{\mu\epsilon\epsilon_0\theta_0}\Big)L^3 \tag{2.14}$$

Thus, the current density is :

$$J = \frac{9}{8}\mu\epsilon\epsilon_0\theta_0\frac{V^2}{L^3} \tag{2.15}$$

Equation 2.15 is similar to Mott-Gurney law given in equation 2.1, except that the current density is decreased by the factor θ_0.

2.2 Frenkel effect

In the absence of a strong applied voltage, the charge carriers might be subjected to electrostatic potential traps, these charge carriers require a minimum energy known as the work function in order to escape through the surface of a given material, which act as a barrier. Unless a strong external electric field (voltage) is applied, those charge carriers in electrostatic potential traps do not contribute to the total current in the device. Frenkel in (1938) and Vermilyea in (1954) discovered that the decrease of the effective depth of a trap may be caused by a strong applied electric field [14]. By considering electron traps as a positively charged centre located in a fixed position in a structureless dielectric, one can write the potential energy of the electron as :

$$V(r) = -\frac{e^2}{4\pi\epsilon\epsilon_0 r} - eEx \tag{2.16}$$

Where E is the electric field along the x-direction. The maximum value of this potential energy is zero ($V(r) = 0$) in the absence of the applied external field and that occurs at $r = \infty$. In the presence of applied external field, $V(r)$ get decreased on one side of the trap (see Fig. 2.2). Now the maximum potential of the trap occurs at a distance x_1 from the trap. The differentiation of equation 2.16 with respect to x gives :

$$\begin{aligned} \frac{dV}{dx} &= -\frac{e^2}{4\pi\epsilon\epsilon_0}\frac{d}{dx}\Big(\frac{1}{x}\Big) - eE \\ \frac{dV}{dx} &= \frac{e^2}{4\pi\epsilon\epsilon_0 x^2} - eE \end{aligned} \tag{2.17}$$

By applying the condition $\frac{dV(r)}{dx} = 0$ at $x = x_1$ (see Fig. 2.2) into the last equation of equations 2.17, and solve for x_1 we get

$$\begin{aligned} \frac{e}{4\pi\epsilon\epsilon_0 x_1^2} &= E \\ x_1 &= \sqrt{\frac{e}{4\pi\epsilon\epsilon_0 E}} \end{aligned} \tag{2.18}$$

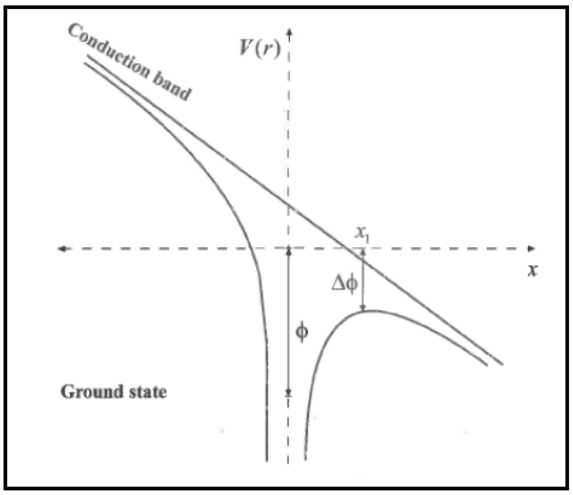

Figure 2.2: The Frenkel effect showing the trap depth ϕ reduced by $\Delta\phi$ [14].

The potential at the point x_1 is calculated as :

$$\begin{aligned} V(x_1) &= \frac{-e^2}{4\pi\epsilon\epsilon_0\Big(\frac{e}{4\pi\epsilon\epsilon_0}\Big)^{\frac{1}{2}}} - eE\Big(\frac{e}{4\pi\epsilon\epsilon_0 E}\Big)^{\frac{1}{2}} \\ &= -\Big(\frac{e^3E}{\pi\epsilon\epsilon_0}\Big)^{\frac{1}{2}} \end{aligned} \tag{2.19}$$

The trap potential is considered to be reduced by this amount $V(x_1) = -\Big(\frac{e^3E}{\pi\epsilon\epsilon_0}\Big)^{\frac{1}{2}}$, and consequently the proportion of carriers, which are free is increased [14]. This equation 2.2 can be written as :

$$\begin{aligned} \frac{\rho_f}{\rho_f+\rho_t} &= \frac{N_c}{N_t} exp\Big(-\frac{A}{kT} + \frac{1}{kT}\Big(\frac{e^3E}{\pi\epsilon\epsilon_0}\Big)^{\frac{1}{2}}\Big) \\ &= \Theta exp\Big(\beta E^{\frac{1}{2}}\Big) \end{aligned} \tag{2.20}$$

Where

$$\beta = \frac{1}{kT}\Big(\frac{e^3}{\pi\epsilon\epsilon_0}\Big)^{\frac{1}{2}} \tag{2.21}$$

If the exponent $\beta E^{\frac{1}{2}}$ is of order unit or greater, that is where the importance of the Frenkel effect is likely to have observable consequences [14].

2.3 Space charge current with Frenkel effect

This section discusses the relation between the current density (J) and voltage (V) across the electrodes with the inclusion of the Frenkel effect. The analysis begins with solving equation 2.3, 2.4 and 2.20 together as follows,
Equation 2.3 and 2.4 can be re-written as :

$$\begin{aligned} \rho_f &= \frac{J}{\mu E} \\ \rho_f + \rho_t &= \epsilon\epsilon_0 \frac{dE}{dx} \end{aligned} \tag{2.22}$$

Elimination of ρ_f and ρ_t by substituting equations 2.22 into equation 2.20 lead us into the following equations :

$$\begin{aligned} \frac{\frac{J}{\mu E}}{\epsilon\epsilon_0 \frac{dE}{dx}} &= \theta_0 exp\Big(\beta E^{\frac{1}{2}}\Big) \\ \frac{J}{\mu E} &= \epsilon\epsilon_0\theta_0 exp\Big(\beta E^{\frac{1}{2}}\Big)\frac{dE}{dx} \\ J &= \mu\epsilon\epsilon_0\theta_0 exp\Big(\beta E^{\frac{1}{2}}\Big)E\frac{dE}{dx} \end{aligned} \tag{2.23}$$

The final equation of equations 2.23 can now be integrated in order to obtain the J-V relation :

$$\begin{aligned} \frac{Jdx}{\mu\epsilon\epsilon_0\theta_0} &= exp\Big(\beta E^{\frac{1}{2}}\Big)EdE \\ \frac{J}{\mu\epsilon\epsilon_0\theta_0}\int dx &= \int exp\Big(\beta E^{\frac{1}{2}}\Big)EdE \end{aligned} \tag{2.24}$$

$$\frac{Jx}{\mu\epsilon\epsilon_0\theta_0} = \int exp\Big(\beta E^{\frac{1}{2}}\Big)EdE \tag{2.25}$$

After several steps of integration by parts of the right hand side of equation 2.25 and taking the arbitrary constant $C = 6$, the following equation is found which is similar to the one reported by Frank and Simmons in 1967 for the first time which results in [14] :

$$\frac{Jx}{\mu\epsilon\epsilon_0\theta_0} = \frac{2}{\beta^4}\Big[exp\Big(\beta E^{\frac{1}{2}}\Big)\Big(\beta^3 E^{\frac{3}{2}} - 3\beta^2 E + 6\beta E^{\frac{1}{2}} - 6\Big) + 6\Big] \tag{2.26}$$

When $\beta E^{\frac{1}{2}}$ is allowed to approach zero, the equation 2.26 tends to equation 2.15. It is not possible to do the analytical integration into equation 2.26 in order to obtain the J-V relation, the solution was found numerically by Murgatroyd in (1970) using Simpson's Rule to a good approximation as [14] :

$$J = \frac{9}{8}\mu\epsilon\epsilon_0\frac{V^2}{L^3}\theta_0 exp\Big[\frac{0.891}{kT}\Big(\frac{e^3V}{\pi\epsilon\epsilon_0 L}\Big)^{\frac{1}{2}}\Big] \tag{2.27}$$

2.4 Chemical and Physical properties of conducting polymers

Organic semiconductors are known as conjugated polymers consisting of alternating single and double bonds in their chemical structure (Fig. 2.3). The backbone of the molecular structure is composed of covalent carbon bonds which are sp^2-hybridized and therefore they possess a π atomic orbital. The overlap of these π orbits along the backbone form delocalized π molecular orbitals, which define the Highest Occupied Molecular Orbital (HOMO) and Lowest Unoccupied Molecular Orbital (LUMO) electronic levels. The optical and electrical properties of the macro-molecules are determined from the difference between HOMO and LUMO levels. The overlap of the HOMO and LUMO π molecular orbitals between the adjacent molecules or polymer chains characterizes the military capability of the intermolecular electronic couplings, which exemplify the key parameter controlling charge carrier mobilities. In crystalline inorganic semiconductors, the three dimensional character and rigidity of the lattice ensure wide valence and conduction bands, and large charge carrier mobilities (typically of the order of 10^2 to 10^3 $cm^2V^{-1}s^{-1}$). In organic semiconductors, the electronic couplings are weak (due to their intermolecular character), the large electron-vibration couplings

(leading to geometry relaxations), and the disorder effects all agree together to produce more modest carrier mobilities due to charge carrier localization and formation of polarons [15]. As an outcome, the charge carrier mobilities strongly depend on the morphology of the film, which can shift over several orders of magnitude in the transition from highly disordered films (typically 10^{-6} to 10^{-3} $cm^2V^{-1}s^{-1}$) to highly ordered crystalline materials (> 1 $cm^2V^{-1}s^{-1}$) [15].

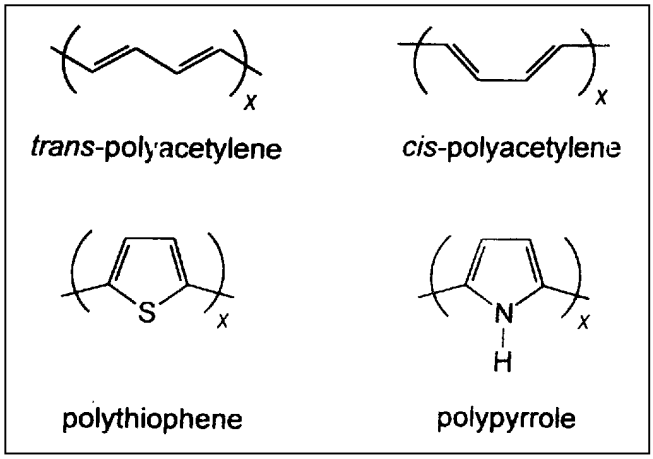

Figure 2.3: Chemical structures of the most common conjugated polymers

Chapter 3

Doping of Conjugated Polymers

The electrical properties of conjugated polymer can be improved by several orders of magnitude by the process of doping the pristine polymers. Doping is a process whereby the electrons are added to or subtracted from the backbone of the conjugated chain with simultaneous insertion of the compensating counter ions between the chains. There are many ways of doping the conjugated polymers :

1. Chemical doping by charge transfer
2. Electrochemical doping
3. Photo-doping
4. Charge injection at a metal semiconductor interface

3.1 Chemical doping

This type of doping can be done by the process called oxidation or reduction via the interaction of the polymer with either the oxidizing agent or reducing agent. Exposing the polymer to a solution or vapor of the

dopant, that could also result in a chemical doping. The most commonly used oxidizing agents are, iodine, arsenic pentachloride(AsF_5) and nitrosonium hexafluorophosphate($NOPF_6$) while sodium naphtalide is a typically reducing agent. The selection of oxidizing or reducing agent is based on their ability to oxidize or reduce the polymer without lowering its ability to conduct electricity, also without starting side reactions that disturb the conductivity of the polymers. In the process of oxidation, the electrons are removed from the valence band and the positive charges are left behind in the polymer resulting p-type doping. These positive charges are strongly spread over many monomer units in the polymer. These positive charges as well cause a geometry relaxation of the polymer to a more energetically favored conformation. In the reduction process, electrons are added on the half filled valence band of the conjugated polymer, then the polymer is left as n-type doping.

3.2 Electrochemical doping

This type of doping can be done by applying an external voltage into a conjugated polymer, typically in a form of a solution. When a positive voltage is applied to the conducting polymer, for exemplar, on an inert electrode, the chemical oxidants or reductants ion moves in from the solution into the conducting polymer towards the sites of the delocalized charge which results in an ionic doping. This anionic doping is named as p-type doping. Likewise, when a negative potential is applied in solution to a conducting polymer immobilized on an electrode, a cation move in from the solution into the polymer. This is named as cationic or n-type doping. The reactions of anionic and cationic doping for poly (pyrrole) (PPy) and poly (p-phenylene)

P(PP) are given below as

Anionic doping

$$(PPy) + nLiCLO_4 \rightarrow (PPy)^{n+}P(PP)^{(n-)} \tag{3.1}$$

Cationic doping

$$P(PP) + nLi \rightarrow (Li)_n^{(n+)}P(PP)^{(n-)} \tag{3.2}$$

3.3 Photo-doping

Photo-doping is another means of doping technique which can be performed by letting out the polymer into intense radiation, for example a Laser light source. During illumination, the electrons will be withdrawn or added from or to the polymer chain. As in the other doping techniques, this also creates a mid gap state which is commonly known as solitons like in the case of Poly (acetylene). A conjugated polymer in undoped state, or neutral state, is generally called as pristine. The range in which oxidation or reduction doping extends is called the doping level, and is measured as the proportion of dopant ions per monomer units. A conducting polymer with one dopant anion per four monomer units has a doping level of 0.25 or 25 %. Doping is uniform throughout the polymer, for example, if one chemically analysis a 25 % doping level, this means that for every four monomer units there is one dopant molecules throughout the polymer.

3.4 Charge injection at a metal semiconductor interface

This case of doping has a substantial part in the electrical attributes of organic semiconductor devices, and is sometimes more dominant than charge transport within the organic semiconductor medium. The mechanism of metal to semiconductor contact can be used to describe the charge injection barrier at the contact interface between a metal and an organic material [16]. This supplies the explanation that a potential barrier is caused by the energy competition between the Fermi-level of the metal and the energy band of the organic material [17]. Thus, the usage of metals with sufficient large work function is commonly thought to be the most important ingredient in curbing the potential barrier for charge injection.

Chapter 4

Device Structure of OPV

The solar energy can be converted into electrical energy using the organic photovoltaic (OPV) devices. The general device structure of OPV consists of one or several photo-active materials which are sandwitched between the anode and cathode electrodes. Thus, there are three types of device structure in the preparation of OPV, which are single layer, bilayer (double layer) and bulk heterojunction (BHJ) layer.

4.1 Single Layer

The concept of organic solar cell initially started based on single thermally evaporated molecular organic layers sandwitched between two metal electrodes consisting of different work functions. The MIM (metal-insulator-metal) model can be used to explain the behaviour of these devices together with a Schottky barrier formation between lower work function metal and p-type organic semiconductor layer can also be used to explain the behaviour of single layer organic devices [16]. In Fig. 4.1, a single layer device is schematically depicted for the case of Schottky contact at the aluminium contact.

The resulting energy band is bending from the so called depletion region

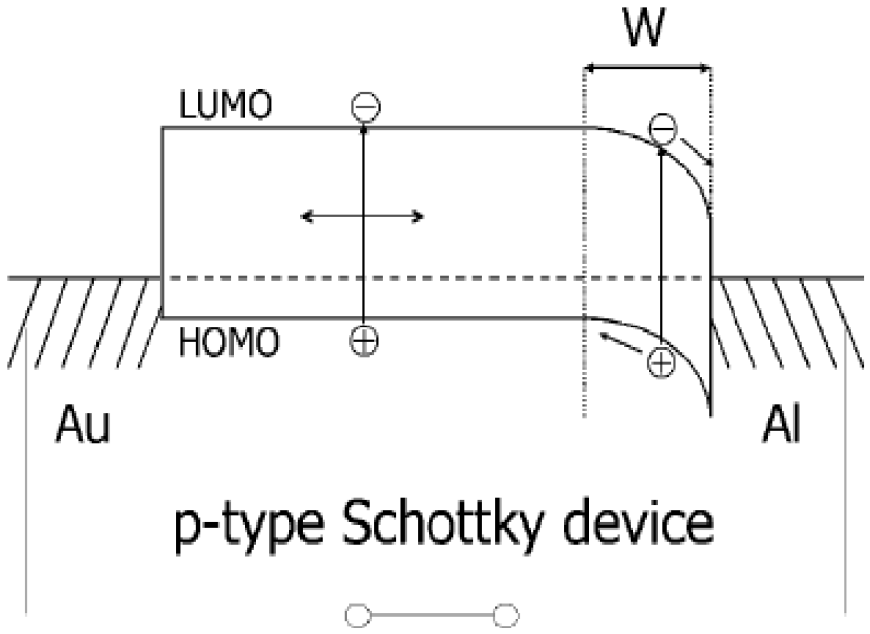

Figure 4.1: Schematic diagram of a Single layer device with a Schottky contact at the aluminium contact [11].

(W). The electric field inside this region correspond to the field required to dissociate excitons. Most of the organic solar cell materials have the exciton diffusion length less than 20 nm, therefore, there are less excitons contributing to the photo-current since they are generated from a small region within $\leq$ 20 nm [4]. The filling factor (FF) in these materials is low and the charge carrier collection depends on the field because of the high series resistances.

4.2 Bilayer Device

In this device structure, the donor and acceptor material is joined together with a planar interface. Here the charge separation takes place at the in-

terface between p-type and n-type layers, which is characterized by a large potential difference between donor and acceptor interface. The bilayer is fitted between two electrodes in such a way that it match the donor HOMO and the acceptor LUMO levels, so that the extraction of the charge carriers will be efficient. The structure of the bilayer device is schematically depicted in Fig. 4.2, ignoring all possible band bending because of energy level alignments. In the bilayer structure, the charge transfer between donor and acceptor of

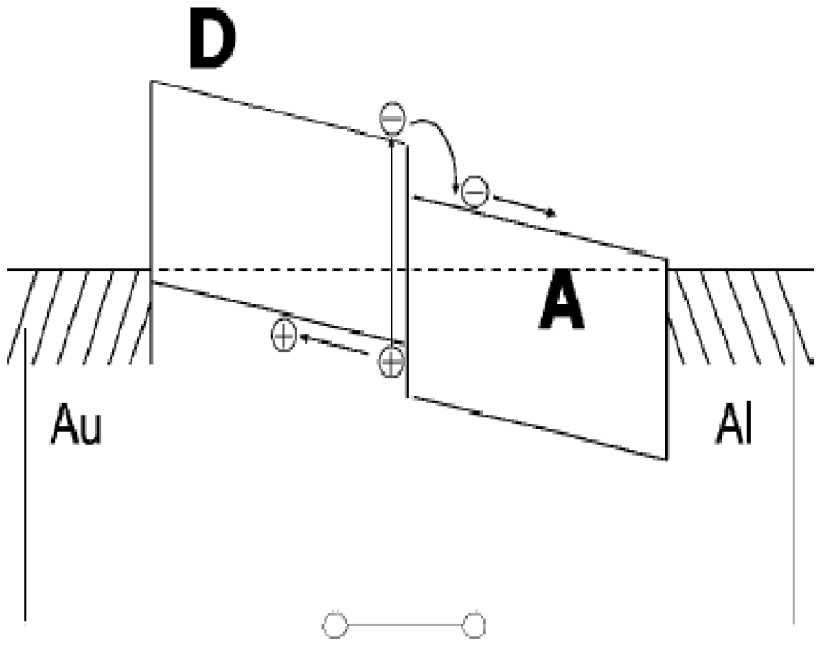

Figure 4.2: Schematic diagram of a Bilayer device where D refers to donor and A refers to acceptor molecules [11].

an undoped material is due to the differences in the ionization potential and electron affinity of the adjacent materials. Although the creation of a classical p/n junction needs doped semiconductors consisting of free charge carriers to create the electric field in the depletion region. The photon is absorbed in the donor (D), then electron get excited from the HOMO to the LUMO. If the

acceptor molecules A is much closer to the donor molecules D, the transfer of electrons to the LUMO of (A) may occur, which is energetically favorable when $I_{D^*} - A_A - U_C < 0$, where I_{D^*} is the ionization potential of the agitated state (D^*) of the donor, A_A is the electron affinity of the acceptor, and U_C is the effective Coulomb interaction [18]. The release of electron energy may then be used to separate electron and hole from their Coulomb potential [4]. It is noted that this charge transfer (CT) occurs only under illumination, as it involves the excitation energy of the donor electron to reach the LUMO in the acceptor. A huge advantage of bilayer over a single layer device is the charge transport. After the dissociation of excitons at the material interface, holes and electrons travel within the p-type donor and n-type acceptor material, respectively. Therefore, electrons and holes are completely separated from each other and therefore charge recombination is highly reduced, as a result, the large FF for thinner layers can be achieved. The power conversion efficiencies for an evaporated bilayer device using copper phthalocyanine and C_{60} [19] were reported about 3.6 % under illumination.

4.3 Bulk Heterojunction

Bulk-heterojunction device active layer is composed of the mixture of donor and acceptor molecules in a bulk volume. In this manner, each donor-acceptor interface has a length which is less than the exciton diffusion length of each absorbing site. Fig. 4.3 shows the bulk heterojunction device schematically, where all kinds of energy level alignments and interface effects are neglected. Bilayer devices and Bulk heterojunction devices are similar to each other with respect to the D-A concept, but bulkheterojunction shows an increased inter-facial area where separation of holes and electrons occurs

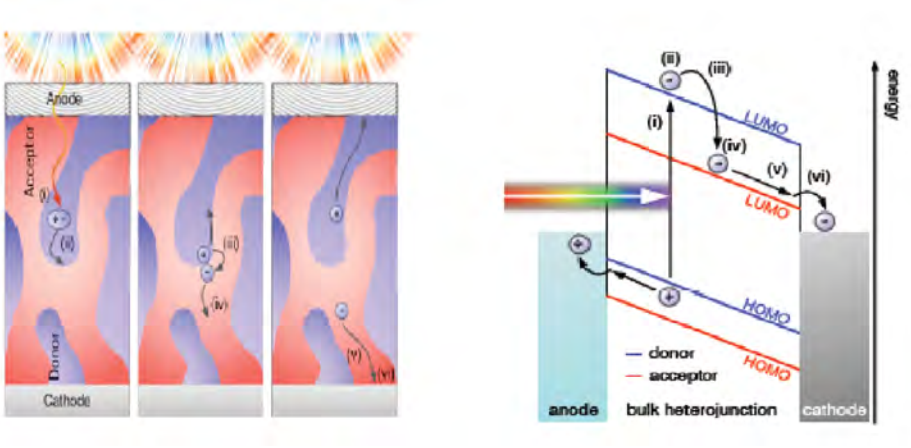

Figure 4.3: Schematic representation of BHJ working principles showing charge generation, dissociation and transportation [20].

at a molecular level. The D-A interfaces are spread throughout the bulk of the photoactive medium, and hence, the photo-generated exciton needs to be dissociated into free charge carriers within their lifetime. In this structure, charges are separated within different phases as in the other device structures, but here the recombination of charges is highly reduced compared to the single and bilayer structures. In the bilayer, the donor phase forms a contact with the anode electrode and the acceptor from a contact with the cathode electrode, but, in the bulk heterojunction the donor/acceptor interfaces spread in the medium creating percolating pathways for transporting holes and electrons to the contacts. Thus, the donor and acceptor must form an interpenetrating network. In general, the bulk heterojunction may be achieved by co-deposition of donor and acceptor pigments [21, 22] or by casting solution of polymer / molecules, or polymer/polymer, or molecule/molecule blend of donor and acceptor. Most of the devices produced today's are based on solution casting P3HT:PCBM blends which results in a η well above 3.5 % [23].

4.3.1 The Origin of Open Circuit Voltage in BHJ

Consider a bulk heterojunction structure composed of a mixture of donor material such as poly(3-hexythiophene) (P3HT) and an acceptor 6,6-phenyl C_{61} butyric acid methyl ester (PCBM). The BHJ medium can be prepared by ways of the solvent based route or dry processing route (co-deposition under vacuum) [24, 25, 2]. There are two specific cases highlighted in this section of the bulk heterojunction structure, which are nonohmic contact and ohmic contact. The energy level alignment given in Fig. 4.4 shows the nonohmic contact. Since there is nonohmic contact, therefore a metal-insulator-metal

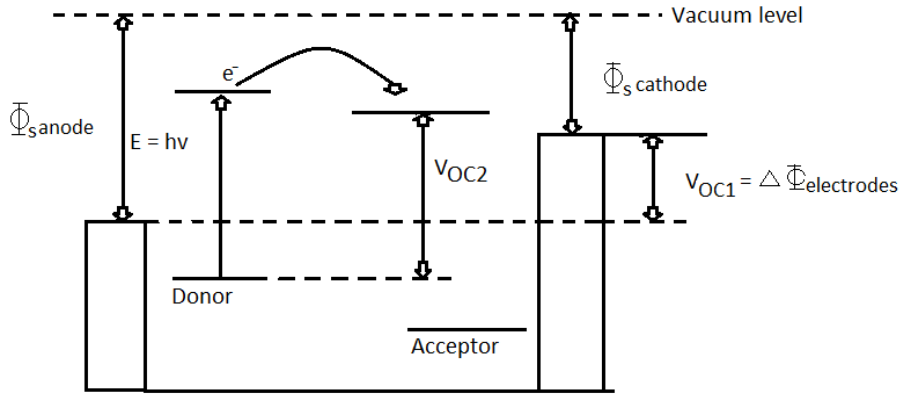

Figure 4.4: Open circuit voltage for bulk heterojunction with nonohmic contact [26].

(MIM) -type behavior is observed, and hence, $V_{OC} = V_{OC1} = \Delta\phi_{electrodes}$.

In the case of ohmic contact (for example on a cathode made from Al or LiF) see Fig. 4.5, the HOMO level of the donor and LUMO level of the acceptor corresponds with the positive and negative electrodes respectively. The maximum V_{OC} is then generally accepted as $V_{OC} = V_{OC2} = E_{LUMO}^{acceptor} - E_{HOMO}^{donor}$. This value is mainly controlled by the bulk material properties. If the Fermi

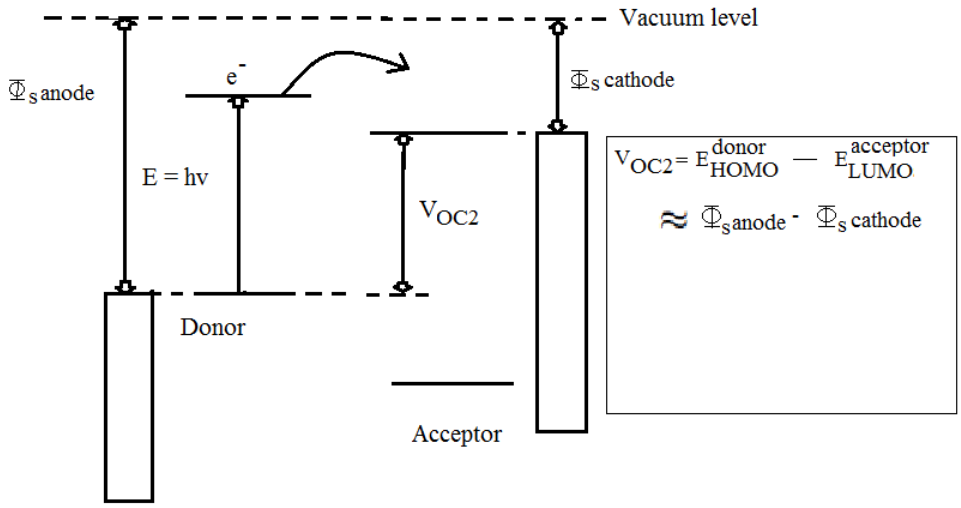

Figure 4.5: Open circuit voltage for bulk heterojunction with ohmic contact [26].

levels of the anode and the cathode are pinned [30] to E_{HOMO}^{donor} and $E_{LUMO}^{acceptor}$ levels then we have $V_{OC2} = E_{LUMO}^{acceptor} - E_{HOMO}^{donor} \approx \phi_{anode} - \phi_{cathode}$.

4.4 Characterization of a Solar Cell

Solar cells can be fabricated from various types of materials which can be classified into two major groups known as inorganic and organic semiconductor materials. Examples of materials often used in the fabrications of solar cells are; gallium-arsenide, silicon, conjugated polymers, etc. However, the organic materials are promising candidates to be used as a cheap photoactive medium for solar cell application. The parameters of a solar cell can be derived from the properties of an ideal solar cell. The ideal solar cell is represented by an equivalent circuit shown in Fig. 4.6. This circuit consist

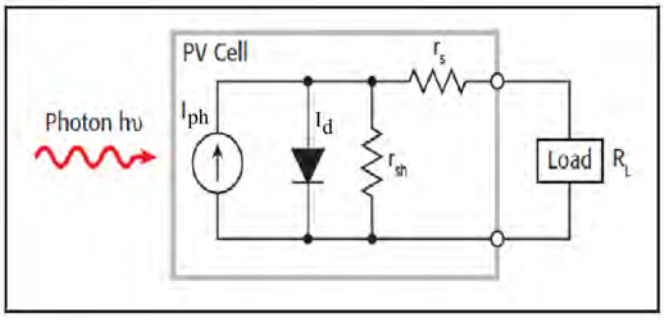

Figure 4.6: Equivalent circuit to an ideal solar cell.

of a current generated by incident photons (I_{ph}), a diode that generates a saturation current, series resistance (r_s), and shunt resistance (r_{sh}). The series resistance is caused by the resistance of metal contacts, junction depth and impurity concentration and it reduces the short circuit current and the maximum power output of a cell. The shunt resistance results from the loss due to the surface leakage on the edge of the cell or to crystal imperfection. There are several parameters used to characterize a solar cell, including η, maximum power (P_{max}) and FF which will be discussed in the next section (section 4.4.1).

4.4.1 Current-Voltage Characteristics of a Solar Cell

In the absence of light illumination, the biased voltage (V) across the MIM junction generates the so called saturation current denoted by I_s. This current is originated by thermal energy, therefore, is also called minority carrier current. Whereas the majority carrier current (which is injection dependent) exponentially grow with applied voltage

$$I_{maj} = I_s.exp(\frac{qV}{kT}) \tag{4.1}$$

Then the resulting measured current density is therefore

$$i = I_s.[exp(\frac{qV}{kT}) - 1] \tag{4.2}$$

When the junction is illuminated with light, there is photocurrent (I_{ph})

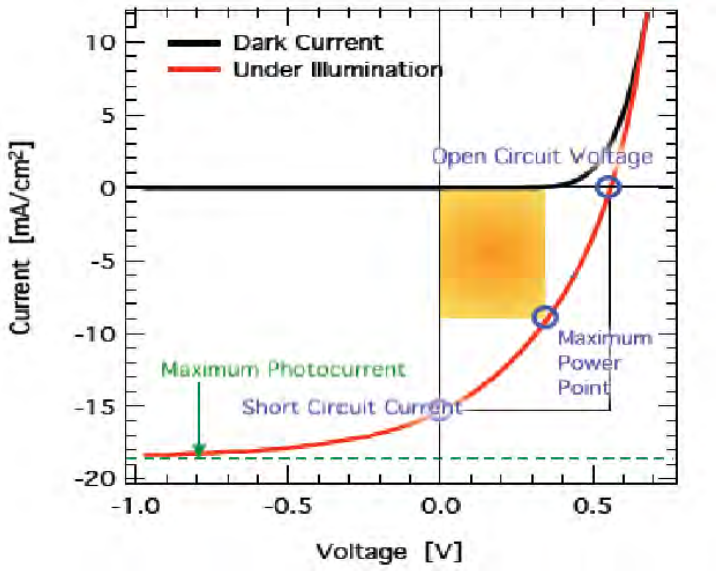

Figure 4.7: Schematic diagram for current-voltage characteristics of a bulk heterojunction solar cell [20].

generated. Therefore, the total current density in the device becomes (see Fig. 4.7)

$$I = I_s[exp(\frac{qV}{kT}) - 1] - I_{ph} \tag{4.3}$$

Under the condition of illumination, the I-V curve does not pass through the origin, and exhibits the following properties:

▶ In the first quadrant, a forward bias $V > V_{OC}$.

▶ In the third quadrant, a photo-diode is under a reverse bias, the current approaches to maximum photo-current exponentially. At $V = 0$, the photo-generated current equals the measured current which is called short circuit

current ($I_{sc} \approx -I_{ph}$).

▶ The product of the voltage and current is negative in the fourth quadrant so that the device can produce the electrical energy equal to the maximum rectangular area formed under the curve. The yellow rectangle in Fig. 4.7 is a maximum power corresponding to the product of the values $I = I_m$ and $V = V_m$ so that

$$P_{max} = V_m I_m \tag{4.4}$$

Therefore, the FF is the ratio of P_{max} to the product of V_{OC} and I_{SC} which are the ratio of the area of the yellow rectangle to that of the white one.

$$FF = \frac{P_{max}}{V_{OC} \times I_{SC}} \tag{4.5}$$

Furthermore, from the current equation 4.3, by substituting $I = 0$ we get the expression for the open circuit voltage as

$$V_{OC} = \frac{kT}{q} log(\frac{I_{ph}}{I_s} + 1) \tag{4.6}$$

From this equation 4.6, it can be seen that the V_{OC} depends on the magnitude of saturation current (I_s). Finally, the η is defined by the ratio of the maximum power to the incident radiant power (P_{in})

$$\begin{aligned} \eta &= \frac{V_m I_m}{P_{in}} \\ &= \frac{(FF)(I_{SC})(V_{OC})}{P_{in}} \end{aligned} \tag{4.7}$$

Therefore, in order to characterize a solar cell, the important parameters such as FF, I_{SC} and V_{OC} must be enhanced.

Chapter 5

Results and Discussion

5.1 Materials and Methods

The binary and ternary bulk heterojunction organic solar cell were fabricated from chloroform based solution. The preparation process begins by etching the ITO coated glass substrate (3 x 3 cm^2), using acid solution containing 48 % HCL, 48 % H_2O and 4 % NHO3 concentrations. After etching, the ultrasonic bath was used to clean the substrate thoroughly by sonicating in detergent, deionized water, acetone and isopropanol for 10 minutes, respectively. The substrates were then dried for 30 minutes in an oven at 150 ^0C.

After the substrate were dried, thin layer of PEDOT:PSS was spin coated on the ITO side of the substrates at 3500 rpm using the spin coater (see Fig. 5.1 a) and then placed in an oven for 30 minutes at 150 ^0C. The photo-active layer composed of a mixture of P3HT:PCBM and P3HT:PTB7:PCBM was prepared separately in chloroform solvent, at stoichiometries ratio of 1:1 and 2:1:1, respectively. The concentration of the solution used was 20 mg/mL. In order to enhance the homogeneity and inter-dispersion of the molecules,

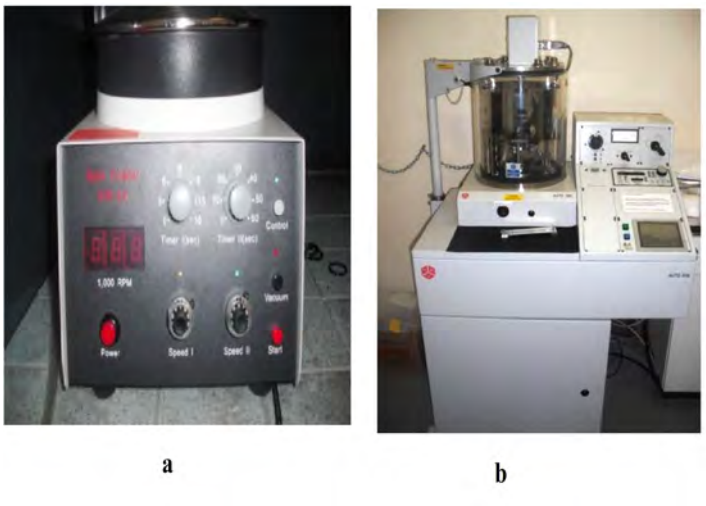

Figure 5.1: (a) PI-KEM LTD Spin Coater KW-4A (b) Edward Auto 306 deposition unit.

the solution was sonicated for three hours at 40 ^0C. The active layers were then spin coated on top of PEDOT:PSS at 1200 rpm for 40 s. The chemical structures of the molecules used are given in Fig. 5.2 . Immediately after

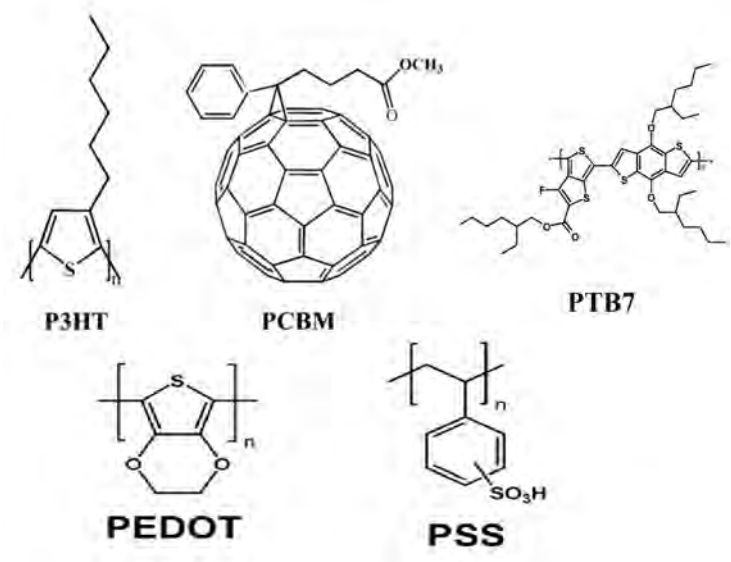

Figure 5.2: Chemical structures of the polymers used [27, 28, 29].

coating the active layer, samples were put into the vacuum chamber Edward Auto 306 deposition unit (Fig. 5.1 b) and finally LiF and Al electrodes were deposited at a base pressure of approximately 2 $\times 10^{-6}$ mbar. The deposition thickness were 0.5 nm for LiF and 60 nm for Al.

5.1.1 Precautions

The cell must be protected from direct exposure to light during the process of fabrication. The dust particles are also needed to be avoided by placing the substrates in a clean container.

5.2 Optical Properties

The difference between the HOMO and LUMO in organic semiconductors represents the energy band gap (E_g) of the material. The low energy photons can be absorbed by low band gap polymers while the high energy photons (UV) can be absorbed by a large band gap polymers. The excess energy from high energy photons will be wasted in the form of heat in the medium. The ternary molecules blend was intended to absorb photons which otherwise cannot be absorbed with binary molecules blend. The organic polymers normally have a wider energy band gap than inorganic semiconductors [31], thus organic polymers produce an efficient absorption in the region near the UV part of the energy spectrum. In this experiment, we studied the optical absorption spectra of the two binary molecules blends P3HT:PCBM and PTB7:PCBM as well as the ternary molecules blend P3HT:PTB7:PCBM using UV-VIS double beam spectrometer. The medium has an efficient absorption near UV region of the energy spectrum, see Fig. 5.3. The binary molecules blend P3HT:PCBM absorb electromagnetic radiation in the region

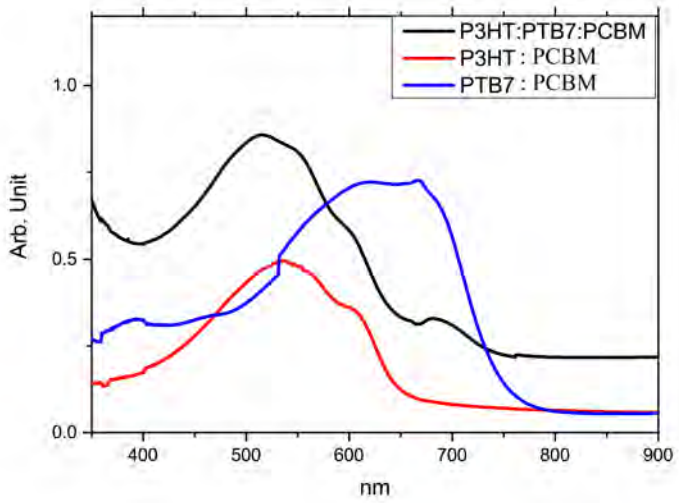

Figure 5.3: Optical absorption spectra of the two bi-molecules blends (P3HT:PCBM and PTB7:PCBM) and one ternary molecules blend (P3HT:PTB7:PCBM).

from 400 nm up to 650 nm while PTB7:PCBM absorb electromagnetic radiation from nearly 400 nm up to 750 nm. According to Fig. 5.3, the absorption peak for P3HT:PCBM occurs at 525 nm while there is also a shoulder occurring at 590 nm. In comparison, the wavelengths where the absorption peak and the shoulder occurs for P3HT:PCBM are almost the same with those reported in literature [32]. This shoulder is common to P3HT molecule and is caused by inter-chain vibrational and electronic absorptions resulted from a high degree of ordering and strong inter-chain interactions [33]. The two absorption spectra for the binary molecules blends overlap between the region 400 nm and 650 nm, but beyond 650 nm, these absorption spectra are separated since PTB7:PCBM is still absorbing electromagnetic waves up to 750 nm. This binary molecules blend PTB7:PCBM has an absorption peak at around 650 nm, this means that PTB7:PCBM absorb more electromag-

netic waves near the infra-red regions of the spectrum while P3HT:PCBM absorb more electromagnetic waves near the ultraviolet regions of the spectrum. From the onset of absorption peak, the energy bandgab (E_g) was determined using the equation

$$E_g = h\nu = h\frac{c}{\lambda} \tag{5.1}$$

Where $h = 6.626 \times 10^{-34}$ Js is a Plank's constant, $c = 2.998 \times 10^8\ ms^{-1}$ is a speed of light and λ is the photon wavelength. From Fig. 5.3, the wavelength corresponding to the start of the absorption for P3HT:PCBM is $\lambda = 650$ nm, therefore, the energy band gap for P3HT:PCBM is calculated as

$$\begin{aligned} E_g &= \frac{(6.626 \times 10^{-34})(2.998 \times 10^8)}{650 \times 10^{-9}} \\ &= 3.0561 \times 10^{-19}\ \ J \\ &= 1.9\ \ eV \end{aligned} \tag{5.2}$$

Where e is the elementary charge of an electron with value $1.602{\times}10^{-19}$ C. This band gap energy we got is almost the same as the band gap found in P3HT:PCBM film in the literature [31]. For PTB7:PCBM, the cut-off wavelength is $\lambda \approx 750$ nm. Therefore, the energy bandgap for PTB7:PCBM is calculated as in equation 5.2, we found $E_g = 1.7$ eV. The energy band gap for PTB7 was reported to be 1.6 eV according to reference [34] which is favorably close to the measured value in this experiment. The small difference between the values could be due to the presence of PCBM in the medium.

The optical absorption of the medium containing the ternary molecules P3HT:PTB7:PCBM blend were also measured, see Fig. 5.3. This ternary molecules blend absorbs electromagnetic radiation in the visible spectrum and extend to near UV and infra-red regions. That is, the absorbance

starts around from 400 nm up to 800 nm. The strong vibronic shoulder of P3HT:PCBM near 590 nm can be still be recognized in the ternary molecules blend. A small bump in the ternary molecules blend spectrum, around 690 nm is associated with the existence of PTB7 in the film. Since P3HT:PCBM is a wide band gap polymer, so it is dominant near the UV region while PTB7:PCBM polymer has a narrower band gap than P3HT:PCBM and dominate near the infra-red region. From Fig. 5.3, the bandgap of the ternary molecules is also calculated from the onset of absorption at the vicinity of $\lambda \approx 760$ nm (is 1.6 eV).

5.3 Electrical Properties of P3HT:PCBM Bulk Heterojunction PV Cell

Bulk heterojunction organic solar cells are produced in sandwitch type structure where the photo-active layer is located between two electrodes as shown in the schematic diagram (Fig. 5.4). After producing the devices, the electrical properties were studied by measuring the current-voltage curve both under light and dark conditions. The active layers were composed of either binary molecules blend P3HT:PCBM or ternary molecules blend P3HT:PTB7:PCBM. The standard SS50AAA solar simulator and Keithly 2400 source meter were used to study the electrical properties of these devices produced in the laboratory. This study was carried out under illumination and dark conditions where the devices were scanned from -0.2 V to 0.8 V and -3.0 V to 3.0 V, respectively. One of the best samples produced using P3HT:PCBM, was plotted in Fig. 5.5 which shows the J-V characteristics. From Fig. 5.5, V_{oc}, J_{sc}, V_{max} and J_{max} are determined. Then the FF and the η were calculated using these parameters and the equations given in chapter

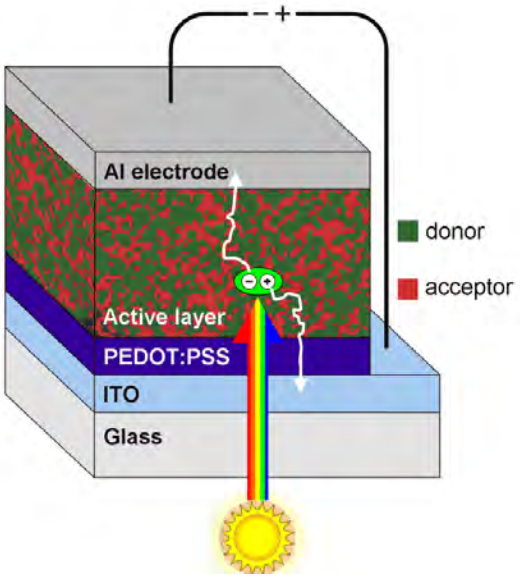

Figure 5.4: Schematic diagram of BHJ photovoltaic cell [35].

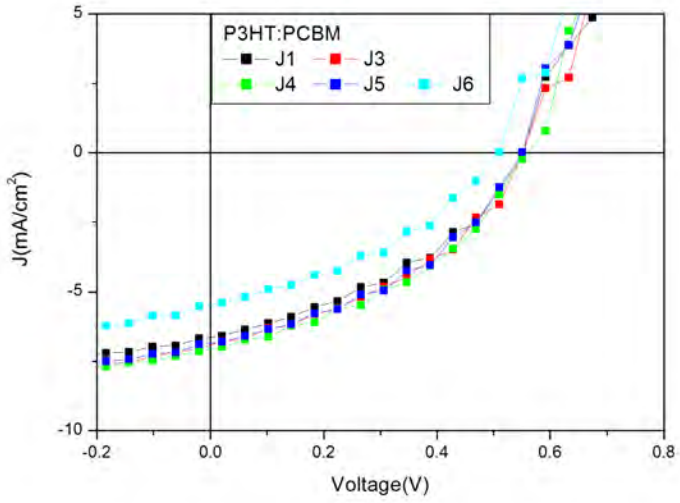

Figure 5.5: P3HT:PCBM device under illumination.

4, equation 4.5 and equation 4.7, respectively. All these parameters are tabulated in Table 5.1. The diodes are required to behave in the same manner but we found diode 6 in this results behaving different from the other diodes in

terms of its open circuit voltage and short circuit voltage. This could result from the exposure time of the device in light during the measurements. All the other diodes except diode 6, they exhibit similar behaviour.

Average η = 1.441 % and Average FF = 39.71 %						
Diodes	$V_{OC}(V)$	$J_{SC}(mAcm^{-2})$	$V_{max}(V)$	$J_{max}(mAcm^{-2})$	FF%	PCE%
diode1	0.5545	6.743	0.3061	4.668	38.21	1.429
diode3	0.5508	6.952	0.3470	4.455	40.37	1.546
diode4	0.5653	7.063	0.3470	4.661	40.50	1.617
diode5	0.5545	6.839	0.3061	4.952	39.97	1.516
diode6	0.5137	5.423	0.3061	3.593	39.48	1.100

Table 5.1: P3HT:PCBM under illumination right after device preparation.

5.4 Ternary Molecules Blend P3HT:PTB7:PCBM Bulk Heterojunction PV Cell

The aim of making the ternary molecules blend P3HT:PTB7:PCBM was to improve the power conversion efficiency and compare these results with standard binary molecules blends P3HT:PCBM discussed in the previous section (5.4). The active layer of the ternary molecules blend was prepared by mixing the solutions of P3HT:PCBM into PTB7:PCBM at 2:1 ratio. The J-V characteristics taken from the ternary molecules blend are given in Fig. 5.6. From Fig. 5.6, one can deduce that, all the diodes are behaving in a different manner in terms of their short circuit current densities and open circuit voltages. By comparing this curve (Fig. 5.6) with the J-V curve of the binary molecules blend P3HT:PCBM (Fig. 5.5) one can deduce that,

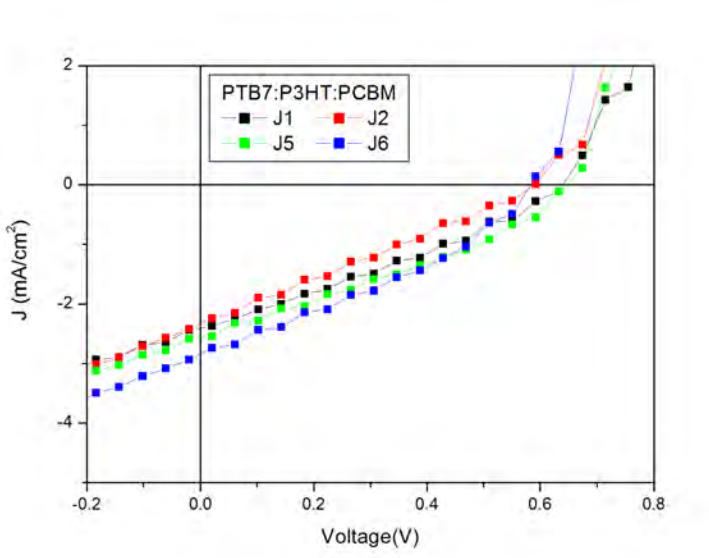

Figure 5.6: P3HT:PTB7:PCBM device under illumination.

P3HT with PCBM alone works better. The averages of the η and FF for the ternary molecules tabulated in Table 5.2 are small compared to that of the binary molecules tabulated in Table 5.1 , which is also one of the reasons why the binary molecules blend of P3HT:PCBM works better than the ternary molecules blend P3HT:PTB7:PCBM.

Average $\eta = 0.4838$ % and Average FF = 30.73 %						
Diodes	$V_{OC}(V)$	$J_{SC}(mAcm^{-2})$	$V_{max}(V)$	$J_{max}(mAcm^{-2})$	FF%	PCE%
diode1	0.6459	2.398	0.3878	1.229	30.77	0.4767
diode2	0.5949	2.296	0.3061	1.229	27.55	0.3763
diode5	0.6460	2.596	0.4286	1.222	31.22	0.5236
diode6	0.5873	2.850	0.3878	1.441	33.37	0.5587

Table 5.2: P3HT:PTB7:PCBM under illumination after 30 minutes.

5.5 Charge Transport Properties of an Organic Solar Cell

The dark currents were measured from the devices by scanning from -3.0 V to 3.0 V under the dark condition. The J-V curves taken under dark condition are given in the Fig. 5.7 below for binary molecules blend and ternary molecules blend. We can see that all the five diodes for the binary

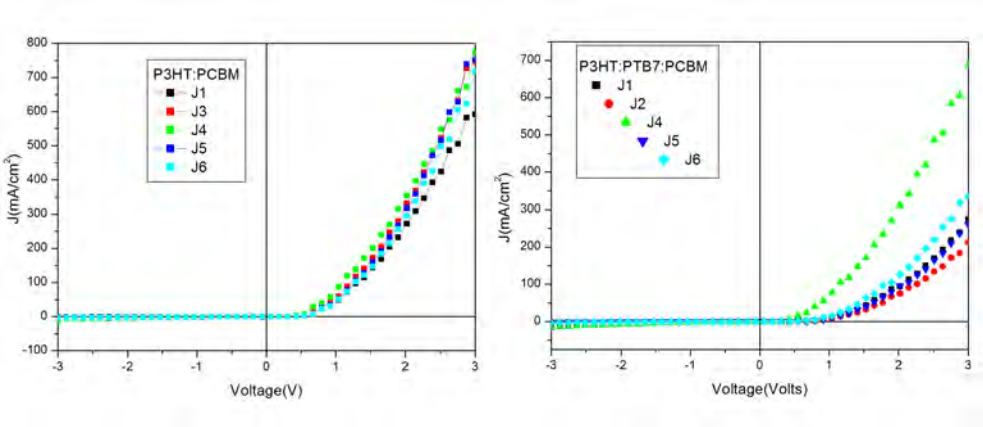

Figure 5.7: Dark current for: (a) Binary molecules blend P3HT:PCBM and (b) Ternary molecules blend P3HT:PTB7:PCBM.

molecules blend are responding in the same manner by looking at the shape of the curve while for the ternary molecules blend one diode is responding differ from the other diodes. These curves do not provide much information about our devices performance, but it is useful for charge transport study. We can see that for a reverse bias, all the diodes produce a negligible amount of current. For a forward bias around $V_{bi} = 1$ Volts, the diodes produces a huge value of the current (current injection) in the case of binary molecules blend, while in the case of the ternary molecules blend, the diodes still produce a small amount of current except for diode 4 which behave the same way

as the diodes of the binary molecules blend. The natural logarithm of the current density was taken in order to find some more information about the devices. This was done by plotting a graph of a natural logarithm of a current density versus the voltages, the graph given in Fig. 5.8 is in the case of binary molecules blend. From this graph (Fig. 5.8), we were able to find some information about the properties of the photoactive medium, such as the zero field mobility (μ_0) and field activation factor (γ). We did proceeded similarly in the case of the ternary molecules blend. According to Fig. 5.8, region 1 consists of a reverse and a forward bias where there is an Ohmic contact behaviour($J \propto V$). Region 2 refers to a current known as injection limited current and increases exponentially with an applied forward bias according to the relation $J \propto exp(\frac{qV}{kT})$. This occurs only when the applied bias is greater than q($\phi_1 - \phi_2$), where ϕ_1 and ϕ_2 are the work functions of the electrodes, then the charge carriers are able to tunnel through the barrier and results to an injection limited current density. This is described in details in terms of Fowler-Nordheim tunnelling theory. Region 3 is a region of interest since it represent SCLC, where the current density is directly proportional to the square of the applied voltage ($J \propto V^2$). In this region, all the traps are filled with the charges and the current becomes very large and reach steady state condition since the injection of charge carriers into a polymer occurs very easily than in the other region. We used the data by region 3, in order to find the important parameters by fitting the logarithm of a Space Charge Limited Current data with SCLC equation. The logarithm of an SCLC used in this experiment was

$$lnJ = ln(\frac{9\epsilon\epsilon_0}{8L^3}) + ln(\mu_0 V^2) + \frac{0.89}{\sqrt{L}}\gamma V^{\frac{1}{2}} \tag{5.3}$$

Where the dielectric constant(ϵ) was chosen to be 3, the permittivity of free space $\epsilon_0 = 8.85 \times 10^{-12}\ Fm^{-1}$, and the thick layer $L = 120$ nm.

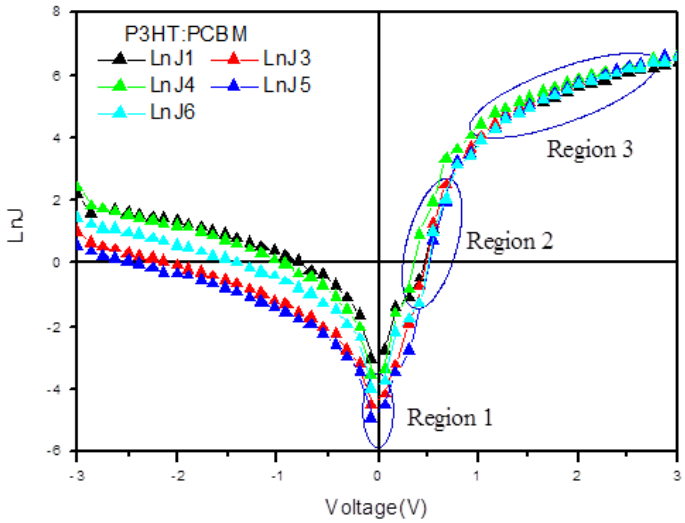

Figure 5.8: Logarithm of the current density versus voltage graph for the binary molecules blend under dark condition.

Fig. 5.9 below shows our experimental data fitted with equation 5.3, and the results confirm that our experimental data are in a good agreement with the theoretical prediction. The zero field mobility (μ_0) and field activation factor (γ) were determined and tabulated on Table 5.3 for P3HT:PCBM. The semi-empirical field dependent mobility equation which is given by $\mu = \mu_0 e^{0.89\gamma\sqrt{E}}$ [36] was used in this experiment to calculate the field dependent mobility (μ) which is also given in Table 6.3. The lowest possible values for the mobility of an organic photovoltaic cells is from the order of magnitude 10^{-6} to 10^{-3} $cm^2V^{-1}s^{-1}$ [37] and the highest possible values can be more than 0.1 $cm^2V^{-1}s^{-1}$ [38]. The average mobility of binary molecules blends P3HT:PCBM in this experiment was found to be 9.527×10^{-5} $cm^2V^{-1}s^{-1}$. This value lies within the range of the lowest possible values of the mobility given above. The same procedure was followed in order to determine the zero field dependent mobility (μ_0), activation factor (γ) and field dependent

Diodes	$\mu_0(cm^2/V.s)$	$\gamma((cm/V)^{\frac{1}{2}})$	$\mu(cm^2/V.s)$
diode1	4.601×10^{-5}	2.400×10^{-3}	8.383×10^{-5}
diode3	4.508×10^{-5}	2.900×10^{-3}	9.308×10^{-5}
diode4	1.092×10^{-4}	8.000×10^{-4}	1.334×10^{-4}
diode5	3.657×10^{-5}	3.400×10^{-3}	8.557×10^{-5}
diode6	3.525×10^{-5}	3.300×10^{-3}	8.045×10^{-5}

Table 5.3: Transport parameters from dark current data of the binary molecules blend P3HT:PCBM.

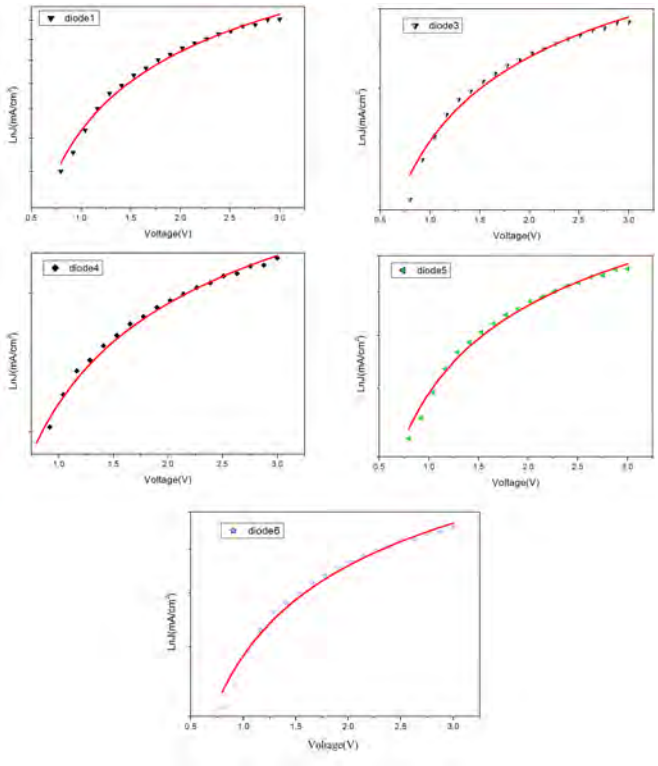

Figure 5.9: SCLC fitted data with equation 5.3 for the binary molecules blend.

mobility (μ) for the ternary molecules blend P3HT:PTB7:PCBM, the results are tabulated on Table 5.4. The average mobility for the ternary molecules blend was found to be 4.880×10^{-5} $cm^2V^{-1}s^{-1}$, it is also within the range of the lowest possible values but less in magnitude compared to the mobility of the binary molecules blends. The low mobility results to a small current of a device, as we can see in this experiment, binary molecules blend has a higher mobility than the ternary molecules blend and is performing better than the ternary molecules blend. According to the charge transport properties [37], our devices produce a good charge mobility. The fitting of equation 5.3 into the dark current data of the ternary blend is also shown in Fig. 5.10 which also shows a good agreement with the theoretical predictions.

Diodes	$\mu_0(cm^2/V.s)$	$\gamma((cm/V)^{\frac{1}{2}})$	$\mu(cm^2/V.s)$
diode1	6.324×10^{-6}	5.000×10^{-3}	2.933×10^{-5}
diode2	5.156×10^{-6}	4.800×10^{-3}	2.249×10^{-5}
diode4	1.280×10^{-4}	5.792×10^{-5}	1.303×10^{-4}
diode5	6.049×10^{-6}	5.000×10^{-3}	2.064×10^{-5}
diode6	1.208×10^{-5}	4.000×10^{-3}	4.123×10^{-5}

Table 5.4: Transport parameters from dark current data of the ternary molecules blend P3HT:PTB7:PCBM.

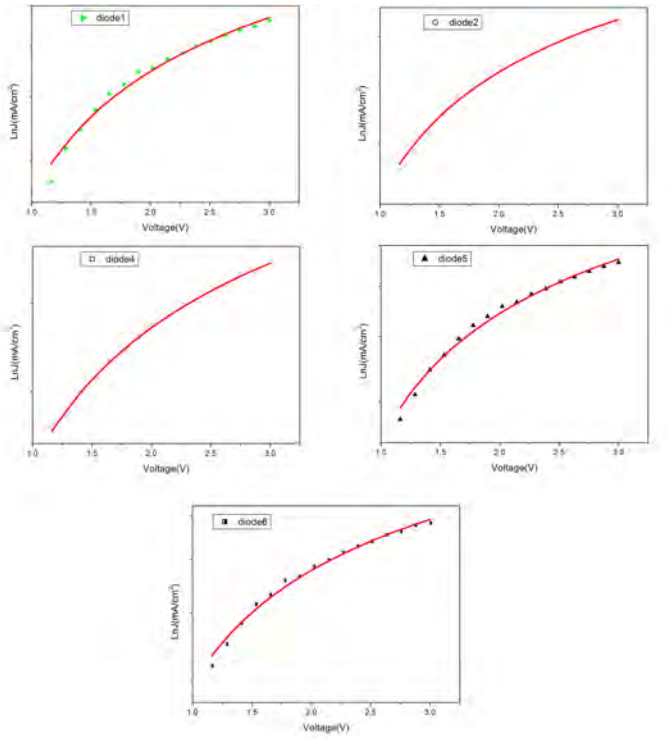

Figure 5.10: SCLC fitted data with equation 5.3 for the ternary molecules blend.

5.6 Morphology of the Active Layer

The investigations of the active layer morphology have been proven to be highly important in determining the optoelectronic properties of the polymer based devices [39]. It plays a significant role in the transportation of the charge carriers. The scanning electron microscopy (SEM) images given in Fig 5.11 shows the morphology of the binary and ternary molecules blend fabricated in this experiment. In Fig. 5.11 (a), the partially white spots are PCBM molecules where the black leaves on top of those white spots are presumably PTB7 molecules, and the dark background moving around those spots in P3HT molecules. In Fig. 5.11 (b), the PCBM molecules

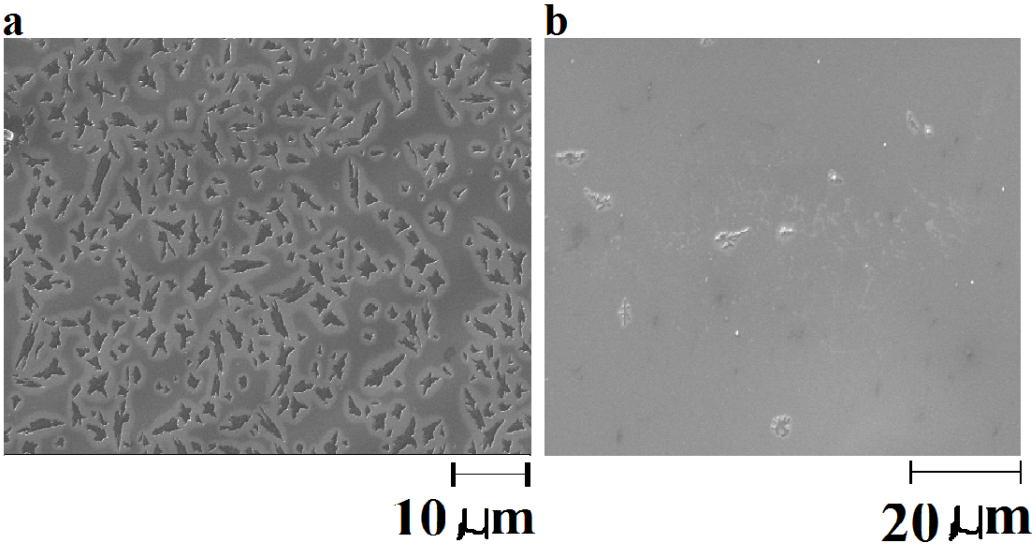

Figure 5.11: Surface morphology (a) P3HT and PTB7 blended with PCBM (b) P3HT blended with PCBM.

(white spots) are distributed randomly in P3HT matrix, which results in increasing the charge separation all over the active layer. The absence of PTB7 molecules in the binary molecules blend leads to the smooth structure of the active layer as we can see from Fig. 5.11 (b).

5.7 Degradation of Binary and Ternary Molecules Blends

Although organic photovoltaic solar cells are promising candidates for mitigating energy problem since the efficiency keep on improving compared to the earlier stage. But, the degradation of an organic solar cell is still another challenge for the researchers. Therefore, in this experiment we investigated the life time of the binary and ternary molecules blends prepared under ambient condition. The samples were tested at different times after the fabrication

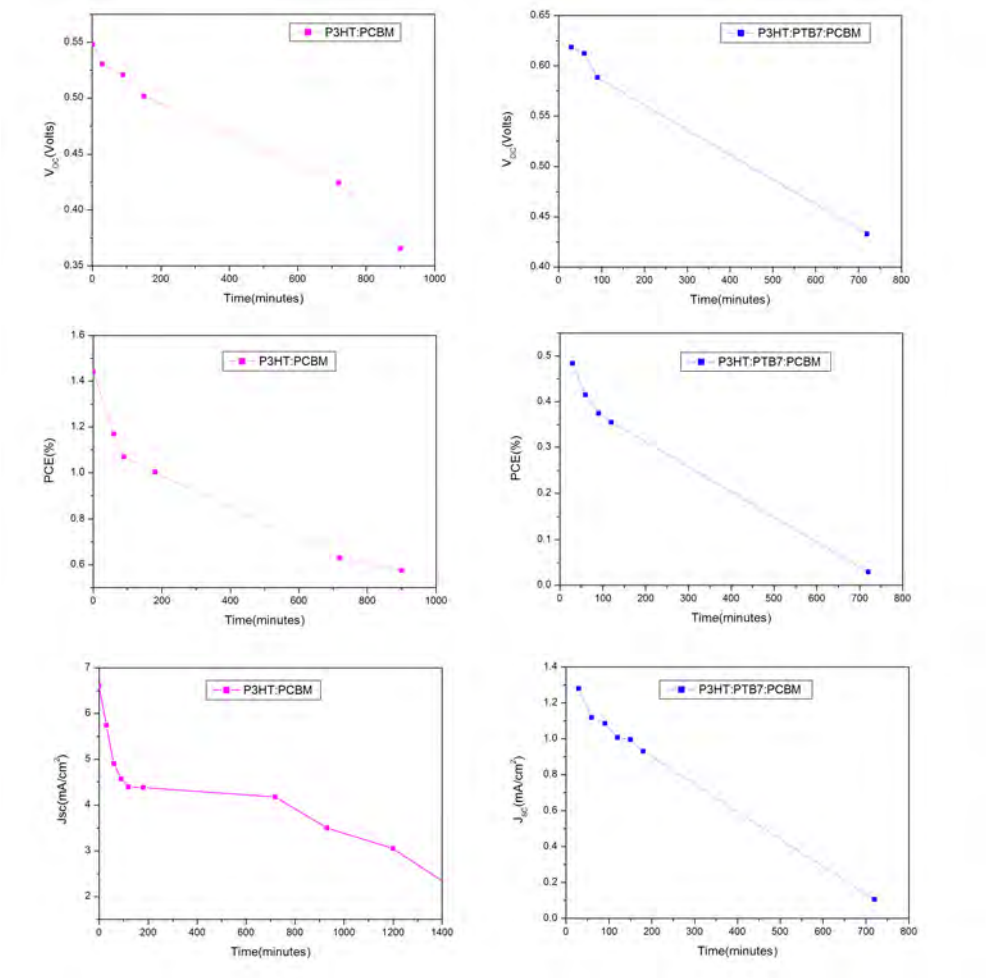

Figure 5.12: Variation of the photovoltaic parameters with respect to time after the fabrication of the devices.

process, where some other diodes were not giving the conclusive results. The samples were covered with a black opaque material to avoid exposure to sunlight while measurements are taken. This was the first step to be met in order to avoid the solar cell to degrade suddenly. The second one is the effect of the humidity during the fabrication of the samples. In Fig. 5.12, parameters of organic solar cells based on binary molecules P3HT:PCBM and the ternary molecules P3HT:PTB7:PCBM blends were plotted against

time. Similar trend of decreasing of solar cell parameters V_{OC}, η, and J_{SC} was observed on both cases as the time elapses. It was observed that for the first three hours after their fabrication, the binary molecules degrade faster than the ternary molecules parameters. The open circuit voltages reduced by about 9 % and 7 % from their initial values for the binary and ternary molecules, respectively, in the first 3 hours. The power conversion efficiency and the short circuit current density showed a drastic loss in the first three hours on both cases binary and ternary molecules. The loss of the efficiency for binary and ternary molecule is about 31 % and 27 %, respectively from its initial value, while the short circuit current density decreases by about 32 % and 29 %, respectively. The operational lifetime of the OPV cells is estimated from Fig. 5.12 to be approximately 12 hours, after 12 hours our samples were not operating efficient. The degradations to our samples are due to absorptions of oxygen and moisture into the organic molecules.

Chapter 6

Conclusion

Organic solar cells based on binary molecules P3HT:PCBM and ternary molecules P3HT:PTB7:PCBM blend were fabricated under the ambient laboratory condition. Immediately after the fabrication process of the samples, electrical properties were studied both under dark and illumination conditions. The results found in this work were in favor of the binary molecule blends compared to the ternary molecules blend. The average power conversion efficiency for the binary molecule was found to be $\eta = 1.441$ %, while in the ternary molecule was found to be $\eta = 0.4838$ %. The poor performance of the ternary molecules blend is associated with low charge mobility in the medium and enhanced charge recombination process. According to the SEM images taken from the two surfaces, one can clearly see the formation of PTB7 clusters on the film containing ternary molecules. The formation of the clusters would hinder the charge transport across the electrode and favorable for charge recombination processes.

Furthermore, the average charge carrier mobilities for binary and ternary molecules found from the data were $\mu = 9.527 \times 10^{-5}\ cm^2V^{-1}s^{-1}$ and

$\mu = 4.880 \times 10^{-5}\ cm^2V^{-1}s^{-1}$, respectively. The optical absorption of the active layers was studied and the band gap energies were calculated from the onset of absorptions and found $E_g = 1.9$ eV for binary molecule blends while for the ternary molecule blends was found to be $E_g = 1.7$ eV.

The devices produced in this work were in a good quality and comparable but less stable with the other results reported in literatures. One thing un-expectable in this work was that the performance of the ternary molecule blends found to be less than that of the binary molecules blend which is contrary to optical absorption result. This work proved that producing organic solar cell can be easy and cheap, however the lifetime and environmental stability of the cell remains as a major challenge to the researchers. From Fig. 5.12 one can deduce that the power conversion efficiency decreased by approximately 33 % after 10 hours exposure to ambient environment.

Bibliography

[1] D. Wohrle and D. Meissner, Organic solar cells, *Adv.Mater*, 3, 129 (1991).

[2] P. Peumans, A. Yakimov and S. R. Forrest, Small molecular weight organic thin-film photodetectors and solar cells, *J.Appl.Phys*, 93, 3693 (2003).

[3] D. L. Morel, A. K. Gosh, T. Feng, E. L. Stogryn, P. E. Purwin, R. F. Shaw and C. Fishman, High efficiency organic solar cells, *Appl.Phys.Lett*, 32, 495 (1978).

[4] G. A. Chamberlain, Organic solar cells: A review, Solar cells, 8, 47 (1983).

[5] C. W. Tang, Two layer organic photovoltaic cell, *Appl.Phys.Lett*, 48, 183 (1986).

[6] M. Hiramoto, M. Suezaki and Yokoyama, Effect of thin gold interstitial layer on the photovoltaic properties of tandem organic solar cells, *Chem.Lett*, 19, 327 (1990).

[7] N.S. Sariciftci, D. Braun, C. Zhang, V.I. Srdanov, A.J. Heeger, G Stucky and F Wuld, *Appl.Phys.Lett*, 62, 585 (1993).

[8] J.C Berned, V Jousseaume, M.A Del Valle, Current trends in polymer sciences.

[9] P.S Revcroft, H Ulal, *Sol.Ener.Mater*, 2, 217 (1979).

[10] H. Shirakawa, C. K. Chiang, Y. W. Park, C. R. Fischer, A. J. Heeger, E. J. Louis, S. C. Gau, A. G. MacDiarmid, *Phys.Rev.Lett*, 39, 1098 (1977).

[11] H. Hoppe and N. S. Sariciftci, Organic solar cells:An overview, *J.Mater.Res*, 19, 1924-1945 (2004).

[12] A. Mozer and N. S. Sariciftci, Conjugated polymer photovoltaic devices and materials, *Chimie*, 9, 568-577, (2006).

[13] S. Gunes, H. Neugebauer, and N. S. Sariciftci, Conjugated polymer based organic solar cells, *Chem.Rev*, 107, 1324-1338 (2007).

[14] P. N. Murgatroyd and H. H. Wills, Theory of space charge limited current enhanced by Frenkel effect, *J.Appl.Phys*, 3, 151-156 (1970).

[15] J.J.M Halls, K Pickler, R.H Friend, S.C Moratti, and A.B Holmes, *Appl.Phys.Lett*, 68, 3120 (1996).

[16] S.M. Sze, Semiconductor Devices, Wiley and Sons, New York, (1981).

[17] H. Ishii, K. Sugiyama, E. Ito and K. Seki, Energy level Alignment and Interfacial Electronic Structures at Organic interfaces, *Adv.Mater*, 11, 605 (1999).

[18] N. S. Sariciftci, L. Smilowitz, A. J. Heeger and F. Wuld, Photoinduced electron transfer from a conducting polymer to buckminsterfullerene, *Science*, 258, 1474 (1992).

[19] P. Peumanns and S. R. Forrest, Very-high efficiency double heterostructure copper phthelocyanine/C_{60} photovoltaic cells, *Appl.Phys.Lett*, 79, 126 (2001).

[20] C. Deibel and V. Dyakonov, Polymer-fullerene bulk heterojunction solar cells, *ReportsonProgressinPhysics*, 73, 096401, (2010).

[21] M. Hiramoto, H. Fujiwara and M. Yokoyama, Three layered organic solar cell with a photoactive interlayer of codeposited pigments, *Appl.Phys.Lett*, 58, 1062 (1991).

[22] W. Geens, T. Aernouts, J. Poortmans and G. Hadziioannou, Organic co-evaporated films of a PPV-pentamer and C_{60}:model systems for donor/acceptor polymer blends, *Thin solid films*, 403, 438-443 (2002).

[23] F. Padinger, R. S. Rittberger and N. S. Sariciftci, Effects of post-production treatment on plastic solar cells, *Adv.Funct.Mater*, 13, 1 (2003).

[24] G. Yu and A. J. Heeger, Charge separation and photovoltaic conversion in polymer composites with internal donor/acceptor heterojunctions, *Appl Phys*, 78, 4510 (1995).

[25] J.J.M. Halls, C.A. Walsh, N.C. Greenham, E.A. Marseglia, R.H. Friend and S.C. Moratti, Efficient photodiodes from interpenetrating polymer networks, *Nature*, 376, 498-500 (1995).

[26] A. Moliton and J. M. Nunzi, How to model the behaviour of organic photovoltaic cells, *Polym Int*, 55, 583-600 (2006).

[27] Y. Teng, Y. Zhang, L. Heng, X. Meng, Q. Yang and L. Jiang, Conductive Polymer Porous Film with Tunable Wettability and Adhesion, *Materials*, 8, 1817 (2015).

[28] M. Thambidurai, J. Y. Kim, Y. Ko, H. Song, H. Shin, J. Song, Y. Lee, N. Muthukumarasamy, D. Velauthapillai and C. Lee, High efficiency inverted organic solar cells with polyethylene oxide modified Zn-doped TiO_2 as an interfacial electron transport layer, *Nanoscale*, 6, 8585 (2014).

[29] M. D. Irwin, p-Type semiconducting nickel oxide as an efficiency enhancing anode interfacial layer in polymer bulk heterojunction solar cells, *PNAS*, 105, 2783-2787 (2008).

[30] H. Ishii, K. Sugiyama and E. Ito, Energy level alignment and interfacial electronic structures at organic/metal and organic/organic interfaces, *Adv Mater*, 11, 605 (1999).

[31] G. Weihao and E. Dagotto, An overview on P3HT:PCBM, the most efficient organic solar cell material so far, Solid State Physics II, Spring (2009).

[32] Y. Shrotriya, K. Emery, G. Li, Y. Yao, T. Moriarty and Y. Yang. Accurate measurement and characterization of organic solar cells, *Advanced Functional Materials*, 16, 2016-2023 (2006).

[33] E. Arbab, B. A. Teleatu and G. T. Mola, Ternary molecules blend organic bulk heterojunction solar cell. Materials science in semiconductor processing, (2015).

[34] S. H. Liao, H. J. Jhuo, Y. S. Cheng and S. A. Chen, Fullerene Derivative-Doped zinc oxide nanofilm as the cathode of inverted polymer so-

lar cells with low bandgap polymer(PTB7-Th) for high performance, *Adv.Mater*, 25, 4767 (2013).

[35] E. Verploegen, R. Mondal, C. Bettinger, S. Sok, M. Toney and Z. Bao, Advanced Functional Materials, 20, 3519-3529 (2010).

[36] O. G. Reid, K. Munechika and D. S. Ginger, Space Charge Limited Current Measurements on Conjugated Polymer Films using Conductive Atomic Force Microscopy, Department of Chemistry, University of Washington, (2008).

[37] H. Sirringhans, P. J. Brown, R. H. Friend, M. M. Nielsen, K. Beckgrand, B. M. W. Langeveld-Voss, A. Spiering, R. A. J. Janssen, E. W. Meijer and P. Herming, Two-dimensional charge transport in self-organized high mobility conjugated polymers, *Nature*, 401, 685-688 (1999).

[38] Z. Bao, A. Dodubalapur and A. J. Lovinge, (1996).

[39] L. Chen, Z. Hong, G. Li and Yang, Recent progress in Polymer Solar cells, Manipulation of Polymer, Fullerene Morphology and the formation of Efficient Inverted Polymer Solar cells, (2009).

[40] S. E. Shohee, C. J. Brabec, N. S. Sariciftci, F. Padinger and J. C. Hummelen, *Appl.Phys.Lett*, 78, 841 (2001).

[41] K. Kim, J. Liu, M. A. G. Namboothiry and D. L. Carroll, *Appl.Phys.Lett*, 90, 163511 (2007).

[42] E. D. Glowacki and C. W. Tang, Department of Chemical Engineering, University of Rochester, USA.

[43] P. Schilinsky, C. Waldauf and C. J. Brabec, Recombination and loss analysis in polythiophene based bulk heterojunction photodetectors, *Appl.Phys.Lett*, 81, 3885 (2002).